Electronic Supplementary Information for

NH_4F-induced morphology-control of hierarchical CoO@MnO_2 core-shell arrays for high performance supercapacitor electrodes

Yin Sun [a], Junjie Zhang [a], Xiannian Sun[a], Naibao Huang*[a]

（College of Transportation Engineering,
Dalian Maritime University, Dalian 116026， China）

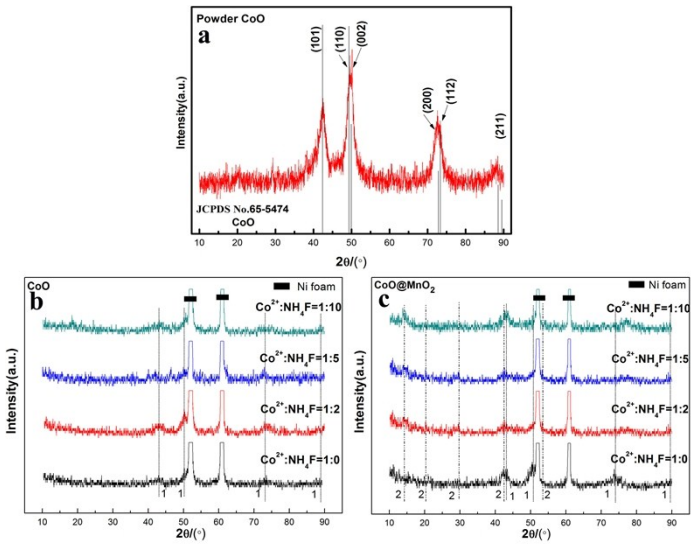

Fig. S1 XRD patterns of different samples. (a) 1:2CoO powder; (b) 1:0, 1:2, 1:5 and 1:10CoO; (c) 1:0, 1:2, 1:5, 1:10CoO@MnO_2 (1represented the diffraction peaks of CoO, 2 represented the diffraction peaks of MnO_2).

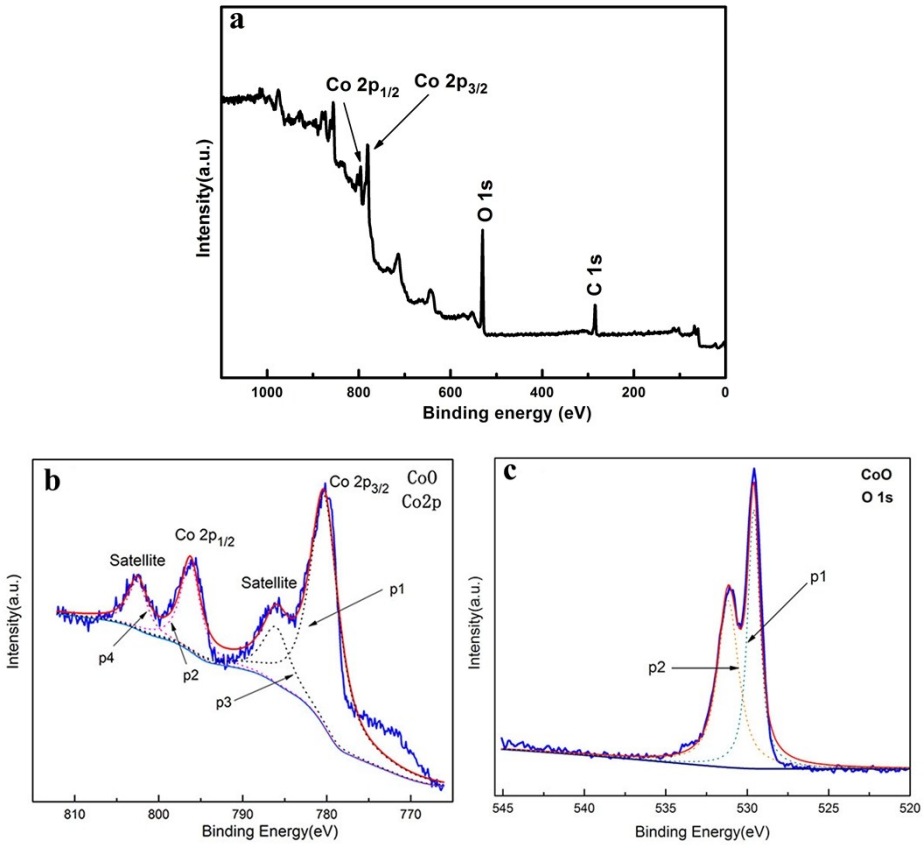

Fig. S2 XPS spectrum of 1:2CoO (a) total survey; (b) Co 2p; (c) O 1s.

As shown in Fig. S2(a), total survey of 1:2CoO mainly consists of C1s, O1s and Co 2p (Co $2p_{1/2}$, Co $2p_{3/2}$). The element signal of NH_4F weren't detected in the total XPS spectrum, which indicated that NH_4F added during the preparation process had been removed from the following washing steps. As showed in Fig. S2(b), the Co 2p of 1:2CoO exhibited two main peaks and two weaker half peaks (marked as satellite peaks), which can be fitted four Gaussian peaks, p1-p4, respectively. The binding energy of p1 and p2 were 780.6 and 796.3 eV, corresponding to the peak of Co $2p_{3/2}$ and Co $2p_{1/2}$, respectively.[1 2] The O 1s spectra (Fig. S2(c)) exhibited two strong peaks, which can be fitted two Gaussian peaks, p1-p2, respectively. The binding energy of p1 and p2 were 529.9 eV and 531.6 eV, corresponding to lattice oxygen of CoO.[3]

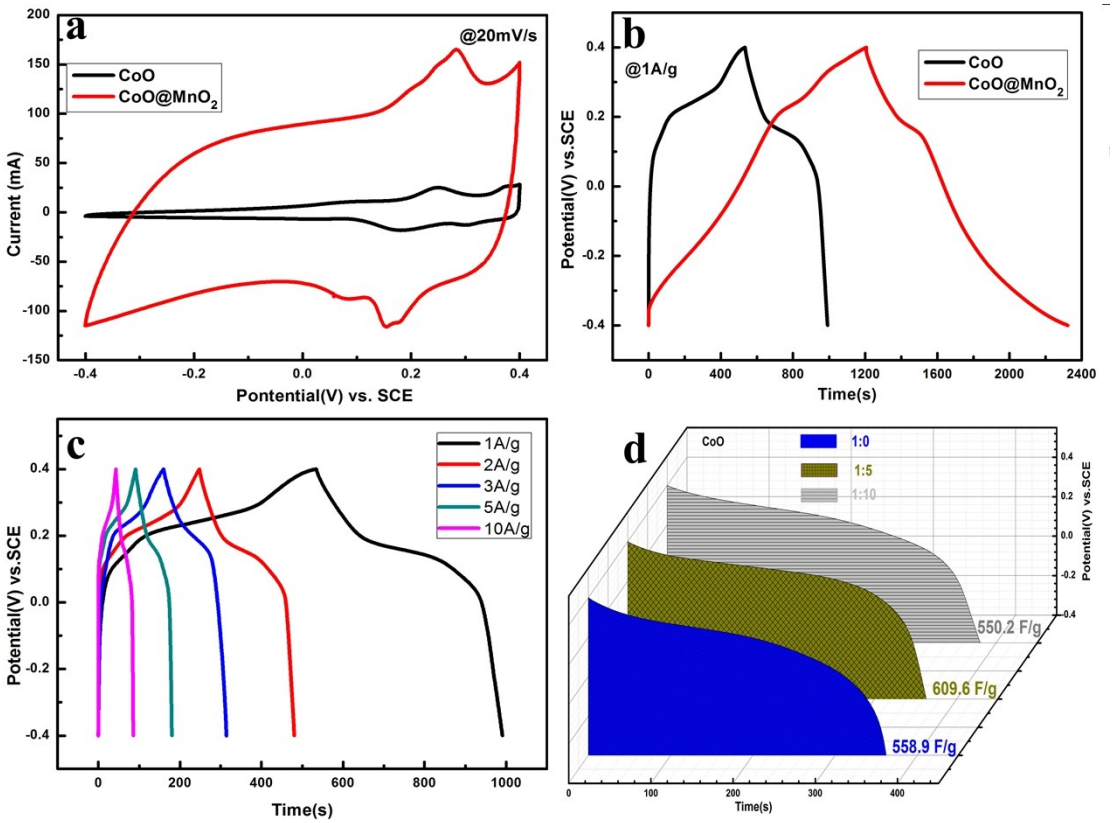

Fig. S3 (a) CV curves of 1:2CoO and 1:2CoO@MnO_2 hybrid at 20 mV/s, (b) GCD curves of 1:2CoO and 1:2CoO@MnO_2 hybrid at 1A/g, (c) GCD curves of 1:2CoO at different current densities, (d) Three-dimensional discharge curves of 1:0CoO, 1:5CoO and 1:10CoO at 1A/g.

Fig. S3(a) shows the CV curves of 1:2CoO and 1:2CoO@MnO_2 hybrid at 20 mV/s. The strong redox peaks were shown in the CV curve of 1:2CoO demonstrated that the capacitance acquisition of CoO electrode was mainly originated by Faradaic redox reaction, which corresponded to the conversion reactions of Co^{2+}/Co^{4+} associated with anions OH^-. [4, 5] The CV of 1:2CoO@MnO_2 hybrid array exhibited similar peaks to CoO, meanwhile, the curve drastically expands and become approximately rectangular. Similar peaks of CoO were shown in hybrid array, indicating the effective utilization of the underlying CoO despite the massive MnO_2 nanosheet covering.[6] The significant increase in the CV integrated area reflected that a much larger capacitance was obtained after the massive MnO_2 nanosheet covering. The shape change to approximately rectangular can be attributed to the presence of MnO_2, which can adsorb electrolyte cations on the electrode surface and suffer from possible intercalation /deintercalation of electrolyte cations.[7]

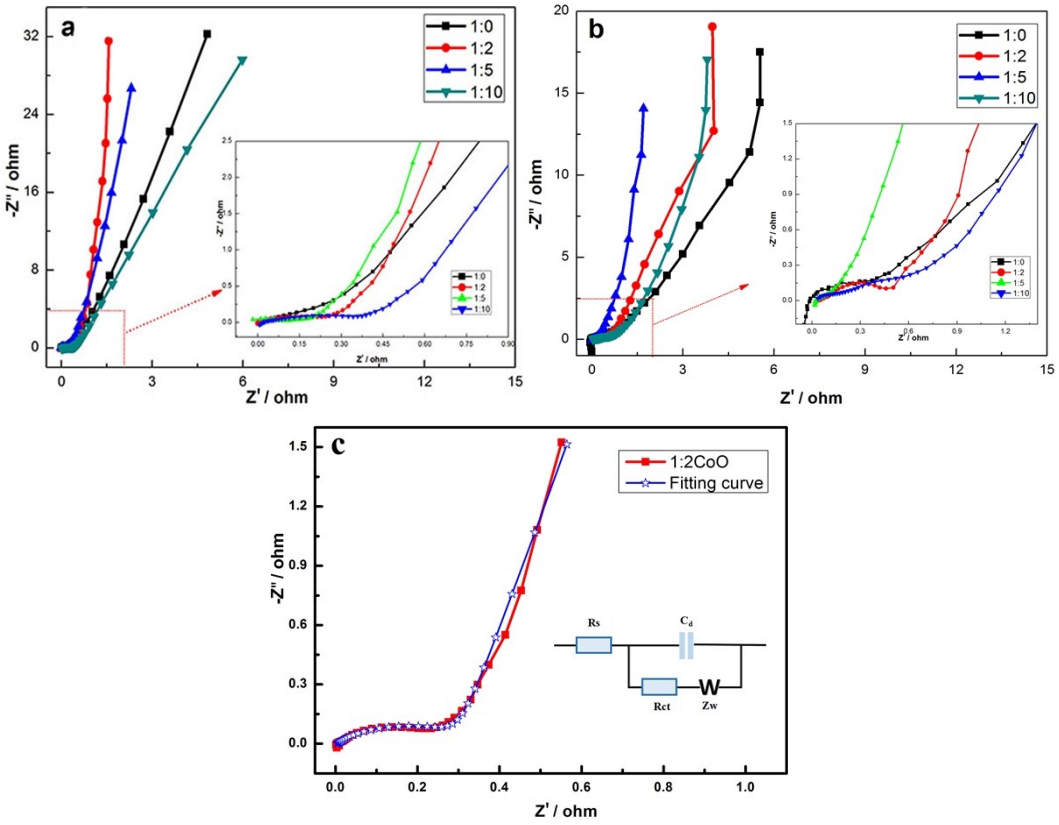

Fig.S4 EIS spectra of (a)1:0, 1:2, 1:5, 1:10CoO; (b) 1:0, 1:2, 1:5, 1:10CoO@MnO_2 hybrids (Insert in (a), (b) show the enlarge-area of the EIS spectra) and (c) EIS spectra of 1:2CoO and the fitting curve (Insert shows the equivalent circuit).

The Nyquist plots and the fitted charge transfer resistance (Rct) of as-prepared CoO and CoO@MnO_2 by adding different concentrations of NH_4F were investigated, as illustrated in Fig.S4, and Tab. S1, respectively. Compared with the pristine CoO electrode, the Nyquist plots of CoO@MnO_2 consisted of a tiny approximate semicircle at the high frequency and followed by a straight line of 45 degree and a vertical straight line at the low frequency. As shown in Tab.S1, compared with CoO electrodes, the CoO@MnO_2 showed a slightly higher charge transfer resistance, causing by the intercalation and deintercalation of cations[8, 9].

Tab.S1 Summary the electrochemical results of different samples.

Sample	**Specific capacitance (F/g)**	**Charge transfer resistance Rct (Ω)**
1:0CoO	550.2	0.361
1:2CoO	668.5	0.303
1:5CoO	609.6	0.226
1:10CoO	558.9	0.485
1:0CoO@MnO_2	1154.2	0.610
1:2CoO@MnO_2	1505.7	0.533
1:5CoO@MnO_2	1363.1	0.217
1:10CoO@MnO_2	1089.2	0.303

Tab.S2 Supercapacitor performances of Mn-based or Co-based core-shell electrode materials reported in recent literatures.

Electrode material	**Specific capacitance**	**Retention**	**Electrolyte**	**ref.**
Co_3O_4 @MnO_2	480 F/g (2.67 A/g)	97.3% (5000 cycles)	1 M LiOH	[10]
NiO@NiO	456 F/g (5 mA/cm^2)	84% (2000 cycles)	6 M KOH	[11]
$MnCo_2O_4$@MnO_2	858 F/g (1 A/g)	88% (5000 cycles)	3 M KOH	[12]
MnO_2@$Ni(OH)_2$	843 F/g (1 A/g)	81% (2000 cycles)	0.5 M Na_2SO_4	[13]
Co@Co_3O_4	1049 F/g (2mV/s)	98% (1500 cycles)	6 M KOH	[14]
$NiCo_2O_4$@$NiMn_2O_4$	539.2 F/g (2 A/g)	93% (5000 cycles)	3 M KOH	[15]
$NiCo_2O_4$@MnO_2	816 F/g (5 mA/cm^2)	81% (5000 cycles)	6 M KOH	[16]
CoO@NiHON	789.3 F/g (1.67 A/g)	95% (2000 cycles)	1 M NaOH	[17]
NiMn@Co_3O_4	607.9F/g (0.5 A/g)	97% (1000 cycles)	6 M KOH	[18]
$CuCo_2O_4$@MnO_2	850 F/g (1 A/g)	94.2% (3000 cycles)	2 M KOH	[19]
MnO_2/$NiCo_2O_4$@N-MWCNT	543 F/g (0.5 A/g)	88% (5000 cycles)	6 M KOH	[20]
CoO@MnO_2	**1505.7 F/g (1 A/g)**	**91.7% (5000 cycles)**	**6 M KOH**	**This work**

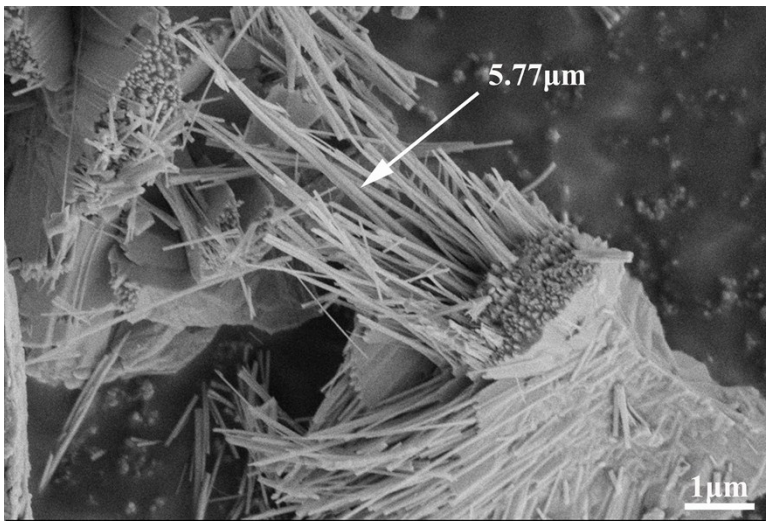

Fig. S5 SEM image of 1:2CoO precursor scraped down from Ni foam obtained during the hydrothermal process.

References

1. D. Barreca, C. Massignan, S. Daolio, M. Fabrizio, C. Piccirillo, L. Armelao and E. Tondello, *Chemistry of Materials*, 2001, **13**, 588-593.
2. Q. Guan, J. Cheng, B. Wang, W. Ni, G. Gu, X. Li, L. Huang, G. Yang and F. Nie, *ACS applied materials & interfaces*, 2014, **6**, 7626-7632.
3. J. Shi, X. Li, G. He, L. Zhang and M. Li, *Journal of Materials Chemistry A*, 2015, **3**, 20619-20626.
4. C. Zhou, Y. Zhang, Y. Li and J. Liu, *Nano letters*, 2013, **13**, 2078-2085.
5. L. Cao, F. Xu, Y. Y. Liang and H. L. Li, *Advanced Materials*, 2004, **16**, 1853-+.
6. J. Liu, J. Jiang, C. Cheng, H. Li, J. Zhang, H. Gong and H. J. Fan, *Advanced Materials*, 2011, **23**, 2076-+.
7. J.-G. Wang, F. Kang and B. Wei, *Progress in Materials Science*, 2015, **74**, 51-124.
8. X. Wang, Y. Xiao, D. Su, S. Xu, L. Zhou, S. Wu, L. Han, S. Fang and S. Cao, *International Journal of Hydrogen Energy*, 2016, **41**, 13540-13548.
9. X. Wang, Y. Xiao, D. Su, L. Zhou, S. Wu, L. Han, S. Fang and S. Cao, *Electrochimica Acta*, 2016, **194**, 377-384.
10. J. P. Liu, J. Jiang, C. W. Cheng, H. X. Li, J. X. Zhang, H. Gong and H. J. Fan, *Advanced Materials*, 2011, **23**, 2076-+.
11. M. Fan, B. Ren, X. Yang, H. Yu and L. Wang, *Journal of Nanoscience and Nanotechnology*, 2019, **19**, 7785-7789.
12. X. T. Zheng, Y. L. Ye, Q. Yang, B. Y. Geng and X. J. Zhang, *Dalton Transactions*, 2016, **45**, 572-578.
13. Z. Y. Wang, F. P. Wang, J. H. Tu, D. Cao, X. X. An and Y. P. Ye, *Materials Letters*, 2016, **171**, 10-13.
14. J. L. Zhang, J. C. Fu, J. W. Zhang, H. B. Ma, Y. M. He, F. S. Li, E. Q. Xie, D. S. Xue, H. L. Zhang and Y. Peng, *Small*, 2014, **10**, 2618-2624.
15. Y. Tian, L. Lin, M. Ning, S. Hussain, H. Su, M. S. Javed, H. Zhen, N. Hu and A. Shaheen, *Ceramics International*, 2019, **45**, 16904-16910.
16. B. Ren, M. Fan, X. Yang, L. Wang and H. Yu, *Chemistryselect*, 2019, **4**, 5641-5650.
17. C. Guan, J. Liu, C. Cheng, H. Li, X. Li, W. Zhou, H. Zhang and H. J. Fan, *Energy & Environmental Science*, 2011, **4**, 4496-4499.

18. H. Peng, C. Jing, J. Chen, D. Jiang, X. Liu, B. Dong, F. Dong, S. Li and Y. Zhang, *Crystengcomm*, 2019, **21**, 470-477.
19. Q. Li, R. Hu, J. Qi, Y. Sui, Y. He, Q. Meng, F. Wei, Y. Ren and Y. Zhao, *Materials Letters*, 2019, **249**, 151-154.
20. A. Kathalingam, S. Ramesh, A. Sivasamy, H. S. Kim and H. S. Kim, *Journal of Sol-Gel Science and Technology*, 2019, **91**, 154-164.